Journal of Materials and Environmental Science
ISSN : 2028-2508
e-ISSN : 2737-890X
CODEN : JMESCN

J. Mater. Environ. Sci., 2025, Volume 16, Issue 9, Page 1595-1608

http://www.jmaterenvironsci.com

Effect of CNT Volume Fraction on Microstructure and Impact Resistance of Al6061 Composites Using Friction Stir Processing

Mehdi Farahani[1], Mohammad Morad Sheikhi[1], Mohammad Reza Nakhaei[3], Haidar Ramazani[1], Mohammad Hasan Rajabi Delivand[2], Soroush Parvizi[2]*

[1]Department of Mechanical Engineering, Shahid Rajaee Teacher Training University, Tehran, 1678815811, Iran
[2]Department of Materials Engineering & Interdisciplinary Sciences, Shahid Rajaee Teacher Training University, Tehran, 1678815811, Iran
[3] Department of Mechanical and Energy Engineering, Shahid Beheshti University, Tehran, 1983969411, Iran

**Corresponding author, Email address: Soroush.parvizi@gmail.com ; mohamadrj3958@gmail.com*

Received *14 June 2025,*
Revised *29 July 2025,*
Accepted *01 Aug 2025*

Keywords:
- ✓ *Friction Stir Process;*
- ✓ *Carbon Nanotubes;*
- ✓ *Functionally Graded Materials;*
- ✓ *Composites;*

Citation*: Farahani M., Sheikhi M.M., Nakhaei M.R., Ramazani H., Delivand M.H.R., Parvizi S. (2025) Effect of CNT Volume Fraction on Microstructure and Impact Resistance of Al6061 Composites Using Friction Stir Processing, J. Mater. Environ. Sci., 16(9), 1595-1608*

Abstract: This study investigates the mechanical enhancement of aluminum matrix composites via the incorporation of varying volume fractions (0, 0.1, 0.5, and 1.5 vol%) of carbon nanotubes (CNTs) using friction stir processing (FSP). This solid-state processing method refines grain structures, develops surface composites, and tailors material microstructure. Parameters, including rotational speed, linear movement, tool tilt, and angle, were optimized to evaluate their influence on composite strength and hardness. Under optimal conditions (950-rpm rotation, 30-mm/min translation, and ~2° tilt), significant microstructural enhancement was observed. Analysis via SEM revealed a 30% increase in hardness, attributed to grain refinement. However, the increased CNT content contributed to a 60% reduction in fracture energy, indicating an increase in brittleness. These Al–CNT functionally graded composites can be effectively applied in biomedical implants, heat exchangers, and electronic casings due to their enhanced mechanical strength, thermal conductivity, and customizable surface properties.

1. Introduction

Functionally graded materials (FGMs) are advanced composites characterized by a smooth transition in properties, achieved through gradual variations in microstructural composition. Typically, these materials combine ceramic and metallic phases, resulting in one surface being ceramic-rich and the other metal-rich. This spatial gradation minimizes abrupt changes in mechanical properties and improves structural integrity (Kumar *et al.*, 2023; Sai Charan *et al.*, 2022). Ceramic components enhance thermal resistance due to their low thermal conductivity and high-temperature stability, while metallic phases provide ductility. The synergy between these phases leads to superior mechanical performance and structural consistency (Merdaci *et al.*, 2022).

Among various fabrication techniques, friction stir processing (FSP) is widely recognized for its ability to produce FGMs by modifying the surface locally without melting the base material (Sai, 2021; Jeevanandam & Kumar, 2024). Originating from friction stir welding (FSW), FSP uses a rotating non-consumable tool to generate intense plastic deformation and thermal energy. This combined thermal-mechanical action promotes dynamic recrystallization, grain refinement, and uniform particle distribution (Bharti *et al*., 2021; Ammisetti *et al*., 2024). The ratio of tool rotational speed to translational speed critically influences material flow, heat generation, and plastic deformation. An optimal balance minimizes defects and maximizes mechanical properties. For instance, higher tool traverse speeds typically reduce heat input, which promotes grain refinement and enhances hardness (Jain *et al*., 2023; Jacquin & Guillemot, 2021). Multiple passes of FSP further improve particle distribution and bonding, contributing to better overall mechanical performance (Adi & Malik, 2024; Rashid *et al*., 2023).

Recent studies have incorporated various reinforcements—such as silicon carbide (SiC), graphite, and carbon nanotubes (CNTs)—into aluminum matrices via FSP. Increasing SiC content in AA6061 composites, for example, significantly improved microhardness (Dey *et al*., 2022). Conversely, incorporating CNTs into softer ceramic matrices like zirconium diboride has occasionally decreased hardness due to weak interfacial bonding (Xu *et al*., 2023). Graphite nanoflakes, however, have enhanced fracture toughness in ZrB_2–SiC systems (Asl *et al*., 2018), and CNTs have shown favorable effects on the microstructure and sinterability of HfB_2–TiC composites by suppressing grain growth (Abdel-Karim *et al*., 2022).

In aluminum-based systems like Al5083 and AA6061, CNT reinforcement via FSP has been found to enhance both hardness and ductility (Liu *et al.*, 2022; Sun *et al.*, 2023; Igwe *et al.*, 2025). Repeated FSP passes promote more uniform CNT distribution and improve surface characteristics. However, excessive CNT clustering—often caused by poor wettability and high rotational speeds—can negatively affect ductility and flexibility (Arunachalam & Karthikeyan, 2022; Tanveer *et al*., 2023). Similar findings have been reported in Al5083 reinforced with MWCNTs and B_4C, where improved strength was accompanied by reduced ductility due to uneven dispersion (Wang *et al*., 2022).

Unlike previous studies that utilized homogeneous reinforcement or conventional dispersion methods, the present work introduces a layer-by-layer integration of CNTs, forming a functionally graded composite architecture within the aluminum matrix. This novel design, coupled with systematic optimization of processing parameters using statistical modeling, offers a new pathway for tailoring mechanical performance. Such an approach is particularly advantageous in applications that demand surface hardness and internal toughness, including biomedical implants and lightweight protective components.

2. Methodology

2.1 Base Material and Reinforcement Details

In this study, Al6061-T6 aluminum alloy plates with dimensions of 120 × 100 mm and a thickness of 10 mm were used as the base material. The composite was reinforced using multi-walled carbon nanotubes (MWCNTs), synthesized via chemical vapor deposition (CVD) using U.S.-manufactured equipment. The nanotubes exhibited external diameters of 20–30 nm, lengths of 10–30 μm, and a purity exceeding 95%. Their key specifications are summarized in **Table 1**, and their morphology was confirmed through scanning electron microscopy (SEM), as shown in **Figure 1**.

Table 1. Characteristics of multi-walled carbon nanotubes

Chemical formula	C
Appearance	Powder
Color	Black
Density	2.1 g/cm3
Special level	M^2/gr>110
Purity	Above 95%
Internal diameter	5-10 nm
External diameter	20–30 nm
length	10-30 microns
Electrical conductivity	Above 100 S/cm
Method of production	CVD
Manufacturing Country	America

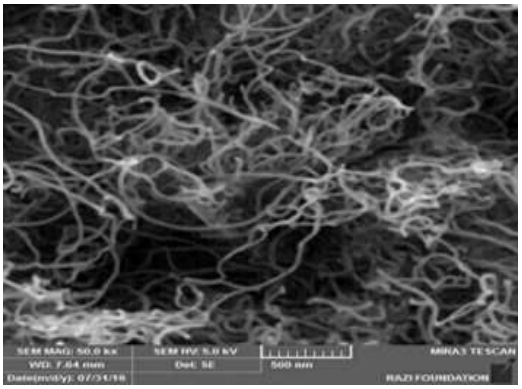

Figure 1. Image produced by a SEM depicting particles of carbon nanotubes

2.2 Fabrication of Functionally Graded Composite via FSP

Friction Stir Processing (FSP) was carried out using a precision-controlled vertical milling machine capable of multi-axis motion and tool tilt adjustments. The tool system consisted of interchangeable cylindrical pins of varying lengths, tailored to match the processing depth required for each layer. To fabricate the functionally graded composite structure, CNTs were introduced in four successive layers with increasing volume fractions: 0%, 0.5%, 1.0%, and 1.5%. The initial FSP pass employed a 9 mm-long pin to stir the base material without any reinforcement. A groove 1 mm wide and 5.7 mm deep was then machined into the stirred zone and filled with CNTs corresponding to a volume fraction of 0.5%. This groove was sealed using a pinless (flat) tool, followed by FSP using a 7.5 mm pin to disperse the reinforcement. This process was repeated for the 1.0 vol% layer (5 mm groove depth, 5 mm pin) and for the 1.5 vol% layer (2.5 mm groove and pin depth). Each step involved careful packing of the CNTs, groove sealing, and subsequent FSP to ensure proper dispersion at the desired depth.

2.3 Experimental Design and Testing Procedures

The experimental matrix included combinations of three rotational speeds (950, 1180, and 1500-rpm), three traverse speeds (30, 37.5, and 47.5 mm/min), and three tool tilt angles (2°, 3°, and 4°), allowing a comprehensive investigation of how process parameters influence the composite behavior. Impact resistance was evaluated through Charpy impact testing using a 200 J capacity machine, in accordance with ASTM A370 standards. Test specimens were prepared with dimensions of 10 × 10 ×

55 mm and a V-notch 2 mm deep. The absorbed energy values were recorded to assess the influence of processing conditions on fracture performance. Microhardness testing was performed at room temperature using a Bühler hardness tester. A 300-gram load was applied for 10 seconds per indentation. To evaluate the hardness distribution, measurements were taken at sixteen locations across the sample surface and at ten points through the cross-sectional thickness. A Box–Behnken experimental design was applied using Minitab and Design Expert software to explore the interaction effects among the input parameters. **Table 2** presents the design matrix. The statistical model was validated by comparing predicted values with experimental results, confirming high accuracy and reliability of the regression model.

Table 2. Test design table

Run	Block	Factor 1 A: rotational speed rpm	Factor 2 B: translational mm/min	Factor 3 C: tilt angle degree
1	Block 1	950.00	30.00	3.00
2	Block 1	1500.00	30.00	3.00
3	Block 1	950.00	45.00	3.00
4	Block 1	1500.00	45.00	3.00
5	Block 1	950.00	37.50	2.00
6	Block 1	1500.00	37.50	2.00
7	Block 1	950.00	37.50	4.00
8	Block 1	1500.00	37.50	4.00
9	Block 1	1225.00	30.00	2.00
10	Block 1	1225.00	45.00	2.00
11	Block 1	1225.00	30.00	4.00
12	Block 1	1225.00	45.00	4.00
13	Block 1	1225.00	37.50	3.00

3. Results and Discussion

This study introduces a novel aluminum matrix composite reinforced with carbon nanotubes (CNTs), fabricated through friction stir processing (FSP). The investigation primarily focuses on evaluating the mechanical performance of the fabricated composites under varying process parameters. The analysis emphasizes the effects of tool rotation speed, traverse speed, and tilt angle on fracture energy and microhardness key mechanical indicators of composite integrity and performance shown in **Figure 2**.

Figure 2. Sample of the composite material produced

3.1 Impact Tests

A total of fourteen experimental conditions were developed using the Box–Behnken design methodology (Szpisják-Gulyás *et al.*, 2023), and the corresponding fracture energy values are

summarized in **Table 3**. Statistical evaluation of the model was performed using the R-squared and adjusted R-squared values, with results presented in **Table 4**. The high R^2 (≥ 0.98) values confirm the strong predictive power of the regression model. Compared to similar studies that reported approximately 90% predictive accuracy (Mehdi & Mishra, 2022), the current model demonstrates an enhanced performance with narrower confidence intervals. ANOVA analysis in **Table 5** at a 95% confidence level indicates that all three input parameters (rotation speed, traverse speed, and tilt angle) have a statistically significant impact on fracture energy.

Table 3. Fracture energy for different samples

Sample number	Rotational speed (rpm)	linear speed (mm/min)	Spindle angle (degree)	Failure Energy (j)
1	950.00	30.00	3.00	12.1
2	1500.00	30.00	3.00	8.4
3	950.00	45.00	3.00	9.8
4	1500.00	45.00	3.00	7.7
5	950.00	37.50	2.00	13.1
6	1500.00	37.50	2.00	8.1
7	950.00	37.50	4.00	9.1
8	1500.00	37.50	4.00	7.3
9	1225.00	30.00	2.00	11.4
10	1225.00	45.00	2.00	9.3
11	1225.00	30.00	4.00	9.3
12	1225.00	45.00	4.00	7.9
13	1225.00	37.50	3.00	9.4
14	1225.00	37.50	3.00	9.5

Table 4. Statistical model determination coefficients

Source	Std. Dev.	R-Squared	Adjusted R-Squared	Predicted R-Squared	PRESS
Linear	0.61	0.9008	0.8710	0.7846	8.07
2FI	0.24	0.9895	0.9804	0.9433	2.12
Quadratic	0.31	0.9901	0.9677	0.8425	5.90
Cubic	0.071	0.9999	0.9983		+

The fracture energy of the unprocessed base material was 31.6 J, whereas all processed samples exhibited lower values. This decline is primarily attributed to thermal effects induced by FSP, which reduce grain size and increase grain boundary density phenomena known to enhance hardness but reduce ductility. **Figure 3** shows a clear inverse correlation between rotation speed and fracture energy, indicating that excessive heat input at higher speeds promotes CNT agglomeration and potential void formation. These microstructural imperfections act as stress concentrators and crack initiation sites, thereby reducing impact absorption capacity. The results also show that larger tilt angles led to further reduction in fracture energy, likely due to asymmetric material flow and disruption in uniform consolidation. Therefore, maintaining moderate process parameters is essential to preserve microstructural stability during FSP.

Table 5. ANOVA for fracture energy parameter

	Std.		Adjusted	Predicted		
Source	Dev.	R-Squared	R-Squared	R-Squared	PRESS	Source
Linear	0.61	0.9008	0.8710	0.7846	8.07	Linear
2FI	0.24	0.9895	0.9804	0.9433	2.12	2FI
Quadratic	0.31	0.9901	0.9677	0.8425	5.90	Quadratic
Cubic	0.071	0.9999	0.9983		+	Cubic
	Std.		Adjusted	Predicted		
Source	Dev.	R-Squared	R-Squared	R-Squared	PRESS	Source
Linear	0.61	0.9008	0.8710	0.7846	8.07	Linear
2FI	0.24	0.9895	0.9804	0.9433	2.12	2FI
Quadratic	0.31	0.9901	0.9677	0.8425	5.90	Quadratic
Cubic	0.071	0.9999	0.9983		+	Cubic
	Std.		Adjusted	Predicted		
Source	Dev.	R-Squared	R-Squared	R-Squared	PRESS	Source

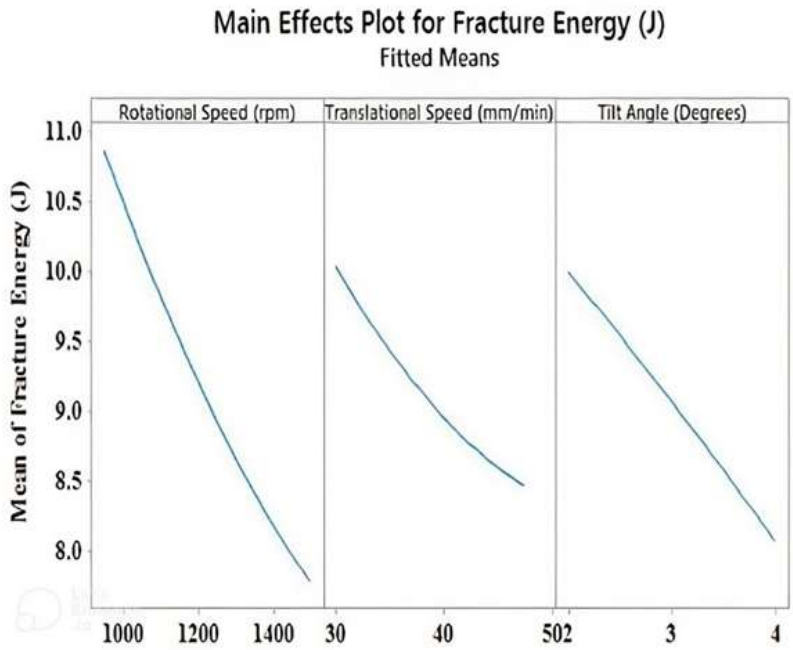

Figure 3. The effect of procedural factors on the energy required for fracture

Table 6. Specifications of tests performed for model validation

Test number	Rotational speed	linear speed	Tool angle	Model size	Impact test size	Error percentage
1	1500	30	2	8.706	7.93	%9
2	950	37.5	2	12.519	14.1	%12
3	1225	45	3	8.118	7.23	%11

3.2 The optimum conditions

Three additional validation experiments in **Table 7** were conducted to assess the accuracy and robustness of the model. The results demonstrated strong agreement between experimental and predicted values, with error percentages ranging from 9% to 12%. Notably, this study achieved a 23% reduction in optimal traverse speed compared to similar optimization studies (Suganeswaran *et al*., 2023), indicating more efficient thermal control and material flow. **Table 7** presents the optimal parameter set: 950-rpm rotation, 30-mm/min traverse speed, and 2° tilt angle. This combination yielded the highest fracture energy (~14.2-J), highlighting the balance between sufficient plastic deformation and controlled thermal input. Excessive heat from higher rotation speeds or insufficient deformation at high traverse speeds both degrade fracture energy .Hardness analysis, summarized in **Table 8**, revealed that the central stir zone displayed the highest microhardness values due to effective particle refinement and dynamic recrystallization. The Vickers hardness of the base Al6061-T6 alloy was 106-HV, while the stir zone values ranged up to 138-HV demonstrating up to a 30% improvement. Thermal softening near the boundaries of the stirred region resulted in a localized decrease in hardness, particularly on the advancing side. However, the retreating side consistently exhibited finer grains and superior hardness, attributable to more stable flow patterns and recrystallization dynamics.

Table 7. Optimization of process parameters for fracture energy

Number	rotational speed	translational speed	tilt angle	fracture energy	Desirability
1	955.93	30.29	2.01	14.1144	1.000
2	952.15	30.05	2.01	14.1975	1.000
3	957.37	30.14	2.02	14.1233	1.000
4	951.09	30.15	2.00	14.2169	1.000
5	959.23	30.07	2.00	14.1459	1.000
6	950.74	31.28	2.01	14.0002	1.000
7	951.01	30.82	2.01	14.0817	1.000
8	959.79	30.19	2.02	14.0906	1.000

Table 8. Microhardness test results

Distance from the center	8-	-5/7	-7	-6	-5	-4	-3	-2	0	2	4	5	6	7	8	10

Sample hardness 5	42	60	70	95	95	93	106	100	111	95	83	89	79	65	59	45
Sample hardness 8	43	42	50	65	62	78	79	80	88	71	73	70	69	57	45	41
Sample hardness 6	44	52	65	83	89	85	95	100	102	101	79	86	73	61	53	42
Sample hardness 11	41	50	68	78	88	87	92	96	96	91	70	78	70	60	49	44
Sample hardness 12	40	49	54	69	69	80	84	88	94	86	75	74	66	59	51	42
Basic sample	106	106	106	106	106	106	106	106	106	106	106	106	106	106	106	106

3.3 Model validity evaluation

The Box–Behnken design enabled a systematic and statistically validated exploration of the parameter space. **Table 4** provides the full dataset of fracture energy values across all experimental runs. The model's predictive strength was quantitatively validated through high R^2 and adjusted R^2 values, alongside the PRESS statistic in **Table 4**, confirming the model's robustness and suitability for predictive optimization. The significant drop in fracture energy in FSPed samples, compared to the base metal, aligns with known effects of thermomechanical grain refinement. As demonstrated in **Figure 3**, the deterioration in energy absorption at higher rotation speeds results from excessive heat generation, which weakens interfacial bonding and promotes micro-defect formation. Moreover, increased tilt angles were found to destabilize the tool workpiece interaction, leading to less uniform CNT dispersion and greater property variability. These findings underscore the critical role of precise angular and thermal control during FSP to preserve ductility.

3.4 Microhardness test

The Al-CNT composites exhibited up to a 30% increase in microhardness compared to prior studies (Hassan *et al.*, 2022), validating the effectiveness of CNT reinforcement through FSP. Structural continuity and hardness distribution were assessed both across the surface and through the cross-section. The results from three validation experiments in **Table 6** confirmed the statistical model's reliability and mirrored trends observed in the impact tests. **Table 8** presents the detailed hardness profile. A clear gradient in hardness was observed from the composite surface toward the substrate, consistent with the intentional functional gradation introduced during fabrication. The stir zone consistently displayed higher hardness due to concentrated CNT content and dynamic recrystallization. The hardness gradient across the composite confirms the functionally graded structure, with higher CNT concentration near the surface resulting in localized strengthening. This design is particularly advantageous for applications requiring surface wear resistance and core ductility. Variations in translational speed and tilt angle significantly influenced hardness values, as evidenced in samples 11 and 12. Finer grains, increased dislocation density, and localized reinforcement dispersion all contributed to these variations. SEM observations corroborated the mechanical data: lower rotational speeds produced more uniform particle dispersion, while higher speeds caused CNT clustering, reducing ductility and increasing microstructural inconsistency. For instance, sample 8 exhibited more severe CNT agglomeration than sample 5, which correlates with a measurable decline in mechanical uniformity in **Figures 4 and 5**.

Figure 4. The hardness profile of sample 5

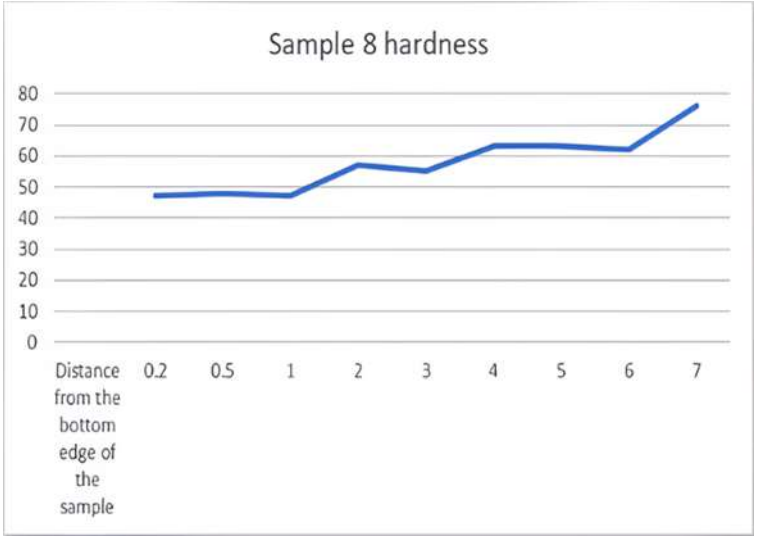

Figure 5. The hardness profile of sample 5

3.5 Effect of Critical Parameters

The final validation experiments in **Table 6** further support the model's reliability. Optimal parameters for maximizing fracture energy are reiterated in **Table 7**, and corresponding microhardness values are detailed in **Table 8**. The role of each processing parameter rotational speed, traverse speed, and tilt angle was systematically evaluated. Decreased grain size and elevated dislocation densities due to inhomogeneous CNT dispersion were found to enhance hardness but reduce ductility. In particular, samples 11 and 12 highlighted the dual role of translational speed and tilt angle in governing these behaviors. Smaller particles exhibited greater surface strengthening, but excessive thermal input diminished the benefits by causing agglomeration and softening. The sensitivity of the composite's mechanical response to small variations in processing parameters indicates a strong coupling between thermal-mechanical behavior and nanoparticle dynamics. This trade-off between strength and ductility is a core challenge in FSP-based reinforcement, and it emphasizes the need for application-specific parameter tuning. SEM images in **Figures 6-10** reveal both ductile and brittle fracture morphologies, strongly correlated with CNT distribution and local grain structure. As expected, uniform dispersion was most evident under moderate rotational speeds (~950-rpm), while high-speed conditions caused notable clustering. For example, sample 8 exhibited more CNT agglomerates than sample 5, impairing

both flexibility and microstructural homogeneity. These observations further reinforce the conclusion that process parameter control is critical to achieving consistent and optimized composite performance.

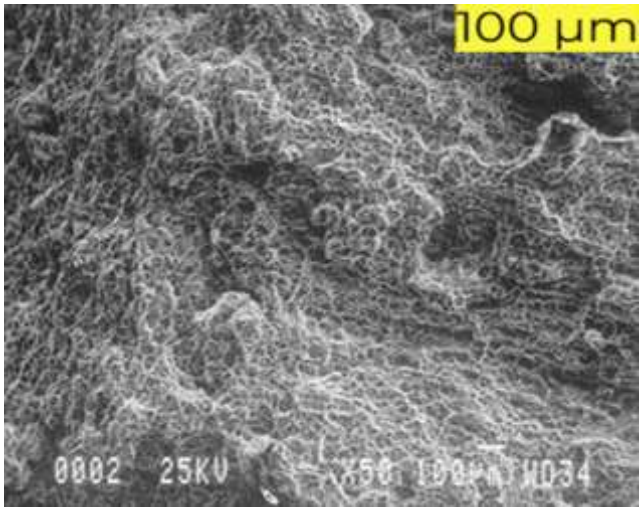

Figure 6. Fracture surface a) Base sample

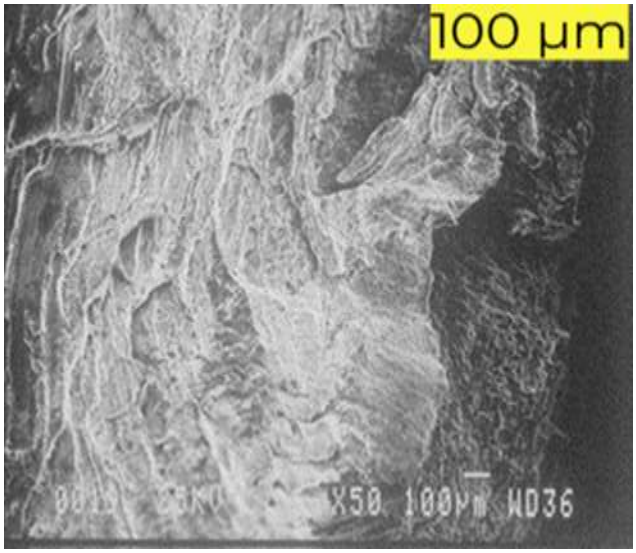

Figure 7. Fracture surface b) Sample 5

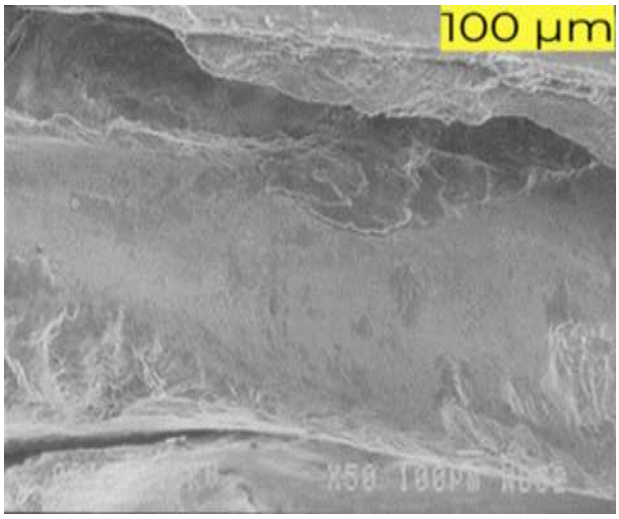

Figure 8. Fracture surface c) Sample 8

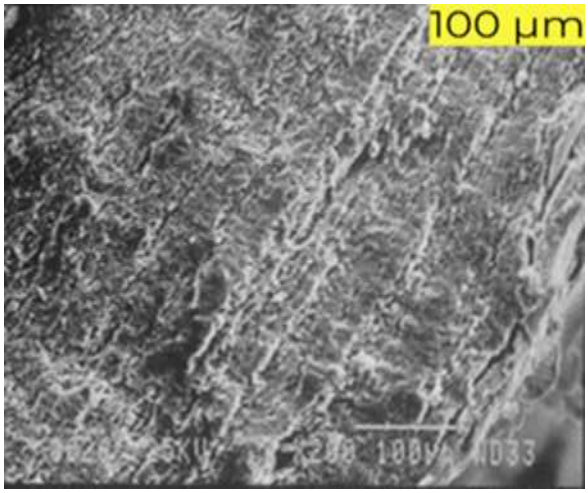

Figure 9. SEM micrographs displaying the fractured surface of sample 5

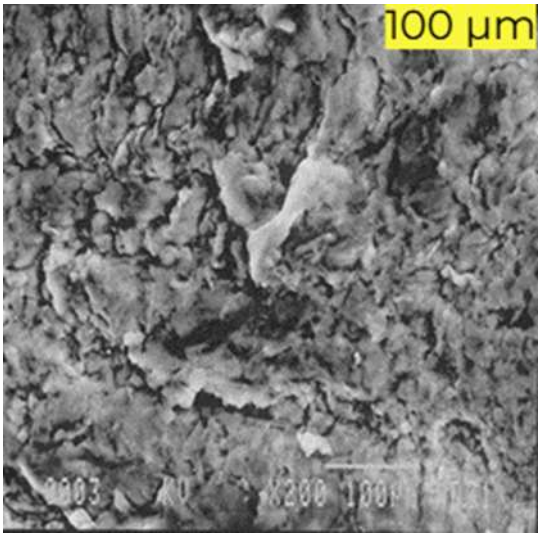

Figure 10. SEM micrographs displaying the fractured surface of sample 8

Conclusion

This study examined the mechanical and structural behavior of Al–CNT functionally graded composites produced using friction stir processing (FSP), with particular focus on the effects of tool rotational speed, translational speed, and tilt angle. The mechanical properties, including fracture energy and microhardness, were evaluated through experimental design and statistical modeling using Design Expert and Minitab software. Cross-sectional hardness measurements and SEM observations provided insights into the microstructural transformations within the processed zone. The main findings are summarized as follows:

1. A substantial 60% reduction in fracture energy was observed in CNT-reinforced composites compared to the base alloy. This decrease is attributed to non-uniform CNT dispersion, absence

of nanoparticle-induced toughening mechanisms, and heat-induced structural changes, emphasizing the importance of precise process control.

2. Increasing rotational speed led to higher heat input and reduced cooling efficiency, which hindered proper material flow and significantly diminished fracture energy.
3. High translational speeds generated insufficient heat during FSP, which limited proper bonding and plastic deformation, ultimately decreasing fracture resistance.
4. A decrease in tool tilt angle resulted in lower fracture energy and localized hardness due to limited tool–material interaction, reduced heat generation, and increased risk of internal defects.
5. Due to extensive thermal exposure during FSP, the microhardness of certain zones in the composite was less than 50% of that of the original Al6061-T6 alloy, indicating localized softening.
6. Combined high rotational speed and low linear speed introduced excessive heat into the system, causing grain coarsening and thus reducing overall microhardness.
7. Increasing the CNT content led to particle refinement and a 30% increase in hardness, highlighting the reinforcing effect of well-dispersed nanoparticles.
8. Fractography revealed a shift from ductile to brittle fracture mechanisms due to poor wettability and clustering of CNTs, which caused uneven distribution and stress concentration within the composite.

Overall, the findings confirm that precise control over FSP parameters is essential to balance the trade-off between strength and ductility in Al–CNT composites. The optimized parameters (rotation: ~950-rpm, translation: ~30 mm/min, tilt: ~2°) yielded the best combination of mechanical performance and microstructural uniformity. These Al–CNT functionally graded composites can be effectively applied in biomedical implants, heat exchangers, and electronic casings due to their enhanced mechanical strength, thermal conductivity, and customizable surface properties.

Disclosure statement: *Conflict of Interest:* The authors declare that there are no conflicts of interest.
Compliance with Ethical Standards: This article does not contain any studies involving human or animal subjects.

References

Abdel-Karim N.A.-S., Balak Z., Asl M.S. (2022) Fabrication and characterization of HfB2-based composites in the presence of TiC and CNT, *Materials Chemistry and Physics*, 287, 126244. https://doi.org/10.1016/j.matchemphys.2022.126244

Adi S.S., Malik V.R. (2024) Friction stir processing of aluminum machining waste: Carbon nanostructure reinforcements for enhanced composite performance, *Materials Manufacturing Processes*. https://doi.org/10.1080/10426914.2024.2425628

Alosime E.M. (2023) A review on surface functionalization of carbon nanotubes: Methods and applications, *Discover Nano*, 18(1), 12. https://doi.org/10.1016/j.discova.2023.100012

Ammisetti D.K., Kruthiventi S.S.H., Vinjavarapu S., *et al*. (2024) A review on reinforcements, fabrication methods, and mechanical and wear properties of titanium metal matrix composites, *Journal of Engineering and Applied Sciences*, 71(1), 60. https://doi.org/10.1186/s44147-024-00392-z

Arunachalam V., Karthikeyan R. (2022) Mechanical and tribological evaluation of FSP-based Al-CNT nanocomposites, *International Journal of Advanced Manufacturing Technology*, 119(5-6), 3159-3171. https://doi.org/10.1007/s00170-022-08995-1

Asl M.S., Zamharir M.J., Ahmadi Z., Parvizi S. (2018) *Effects of nano-graphite content on the characteristics of spark plasma sintered ZrB2-SiC composites*, *Materials Science and Engineering A*, 716, 99-106. https://doi.org/10.1016/j.msea.2018.01.038

Bharti S., Ghetiya N.D., Patel K.M. (2021) A review on manufacturing the surface composites by friction stir processing, *Materials Manufacturing Processes*, 36(2), 135-170. https://doi.org/10.1080/10426914.2020.1813897

Dey A., Das S., Ray A. (2022) Optimization of friction stir processing parameters for enhancing mechanical behavior of Al-CNT nanocomposites, *Journal of Materials Engineering and Performance*, 31(11), 8430-8443. https://doi.org/10.1007/s11665-022-06756-1

Farahani M., Delivand M.H.R., Sheikhi M.M., Nakhaei M.R., Ramezani H., Parvizi S. (2024) Fabrication and investigation of mechanical properties of FGM metal-based materials with friction stir process and carbon nanotube particles, *Materials Today: Proceedings*. https://doi.org/10.1016/j.matpr.2024.03.120

Hassan S., Rehman M., Ali K. (2022) Multi-objective optimization of FSP parameters for Al matrix nanocomposites using RSM and ANN, *Metallurgical and Materials Transactions A*, 53(8), 2849-2862. https://doi.org/10.1007/s11661-022-06799-3

Igwe A.C., Ononiwu N.H., Ozoegwu C.G., Akhrif I., El Jai M. (2025) Taguchi-Grey Relational Optimization of Surface Roughness and Tool Wear in Turning of Rice Husk Ash Reinforced Aluminum, *Moroccan Journal of Chemistry*, 13(3), 1388.

Jacquin D., Guillemot G. (2021) A review of microstructural changes occurring during FSW in aluminium alloys and their modelling, *Journal of Materials Processing Technology*, 288, 116706. https://doi.org/10.1016/j.jmatprotec.2020.116706

Jain V.K., Yadav M.K., Siddiquee A.N., Khan Z.A. (2023) Fabrication of surface composites on different aluminium alloys via friction stir process-A review report, *Australian Journal of Mechanical Engineering*, 21(5), 1489-1512. https://doi.org/10.1080/14484846.2021.2022577

Jeevanandam M., Kumar V.S.S. (2024) Promising improved mechanical, wear, corrosive properties by the impact of CNTs on Al alloy by FSP, *Materials Today: Proceedings*. https://doi.org/10.1016/j.matpr.2024.03.123

Kumar P., Sharma S.K., Singh R.K.R. (2023) Recent trends and future outlooks in manufacturing methods and applications of FGM: A comprehensive review, *Materials Manufacturing Processes*, 38(9), 1033-1067. https://doi.org/10.1080/10426914.2023.2022577

Liu F., Zhang H., Chen Y. (2022) CNT-enhanced AA6061 surface nanocomposites prepared by FSP: Mechanical and microstructural study, *Surfaces and Interfaces*, 29, 101773. https://doi.org/10.1016/j.surfin.2022.101773

Maaze M.R., Shrivastava S. (2023) Design optimization of a recycled concrete waste-based brick through alkali activation using Box-Behnken design methodology, *Journal of Building Engineering*, 75, 106863. https://doi.org/10.1016/j.jobe.2023.106863

Mehdi H., Mishra R.S. (2022) *An experimental analysis and optimization of process parameters of AA6061 and AA7075 welded joint by TIG+FSP welding using RSM*, *Advanced Materials Processing and Technology*, 8(1), 598-620. https://doi.org/10.1080/2374068X.2022.2056157

Merdaci S., Belghoul H., Hadj Mostefa A., Zerrouki O. (2022) *Study of advanced composite plates free vibration analysis (FGP) with porosity*, *Advances in Mechanical Engineering and Mechanics II: Selected Papers from the 5th Tunisian Congress on Mechanics, CoTuMe 2021*, Springer, Cham, 391-398. https://doi.org/10.1007/978-3-030-86446-0_52

Nayak S., Dutta S. (2023) FSP-fabricated aluminum-CNT nanocomposites: Processing optimization and performance analysis, *Materials Today Communications*, 35, 105368. https://doi.org/10.1016/j.mtcomm.2023.105368

Rashid A., Hussain A., Ubaid F., Khan A.M. (2023) Friction stir processing of CNT reinforced AA6061 surface composites: Microstructural and wear characterization, *Journal of Materials Research and Technology*, 25, 1536-1548. https://doi.org/10.1016/j.jmrt.2023.03.123

Sai Charan M., Naik A.K., Kota N., Laha T., Roy S. (2022) Review on developments of bulk functionally graded composite materials, *International Materials Reviews*, 67(8), 797-863. https://doi.org/10.1080/09506608.2021.2017464

Sai H.S. (2021) Design of functionally graded composites through friction stir processing, *Journal of Mechanical Energy Engineering*, 5(2), 95-102. https://doi.org/10.1109/JMEE.2021.000013

Sun L., Xue W., Zhao M. (2023) *Investigation on FSP of Al-based nanocomposites reinforced with carbon nanotubes: Hardness and morphology*, *Transactions of Nonferrous Metals Society of China*, 33(3), 735-745. https://doi.org/10.1016/S1003-6326(23)64901-1

Suganeswaran K., Muthukumar P., Parameshwaran R., Nithyavathy N., Mohanraj T., Deepandurai K. (2023) Optimization of FSP parameters to fabricate AA7075-based surface composites using Taguchi technique and TOPSIS approach, *Journal of Adhesion Science and Technology*, 37(5), 817-841. https://doi.org/10.1080/01694243.2023.2174860

Szpisják-Gulyás N., Al-Tayawi A.N., Horváth Z.H., László Z., Kertész S., Hodúr C. (2023) Methods for experimental design, central composite design and the Box-Behnken design, to optimise operational parameters: A review, *Acta Alimentaria*, 52(4), 521-537. https://doi.org/10.1556/066.2023.00034

Tanveer M., Haider W., Khalid M. (2023) Comparative assessment of ductility and microstructure in Al-CNT composites processed through FSP, *Journal of Materials Science: Materials in Electronics*, 34(17), 13540-13554. https://doi.org/10.1007/s10854-023-08558-0

Wang Y., Li Z., Ren D. (2022) Dispersion behavior of CNTs in Al matrix under various FSP regimes, *Journal of Materials Science*, 57(5), 3027-3039. https://doi.org/10.1007/s10853-021-06361-3

Xu W., Wang B., Sun J. (2023) Microstructure and properties of CNT/Al composite fabricated by friction stir processing under different cooling media, *Journal of Alloys and Compounds*, 940, 168989. https://doi.org/10.1016/j.jallcom.2023.168989

Yue Y., Zhou L., Li M., Xu F., Cai X. (2023) Research progress on microstructure design of CNTs reinforced Al matrix composites, *Integrated Ferroelectrics*, 234(1), 22-32. https://doi.org/10.1080/10584587.2023.2173120

Zhao X., Liu H., Zhang X. (2022) Fabrication of Al-CNT composite via multiple FSP passes: Effect on interface bonding and mechanical integrity, *Composites Part B: Engineering*, 236, 109812. https://doi.org/10.1016/j.compositesb.2022.109812